Numerical Analysis of Sliding Dynamics in Three-Dimensional Filippov Systems using SPT Method

IVAN ARANGO
Universidad EAFIT
Department of Mechanics Engineering
Kra 42d 50 sur 40 Medellín
Colombia
iarango@eafit.edu.co

JOHN ALEXANDER TABORDA
Universidad Nacional de Colombia
Department Electronics Engineering
Campus La Nubia Manizales
Colombia
yatabordag@unal.edu.co

Abstract: We present the numerical analysis of sliding dynamics on the discontinuity boundary (DB) of three-dimensional (3D) Filippov systems using an integration-free method denominated *Singular Point Tracking* (SPT). Many physical applications in engineering can be modelled as Filippov systems. Sliding dynamics due to non-smooth phenomena such as friction, hysteresis or switching are inherent to Filippov systems. The analysis of sliding dynamics have many mathematical and numerical difficulties. Several well-known numerical problems can be avoid using integration-free methods. Three-dimensional Filippov systems are being studied extensively because these systems still have many open problems. In this paper, we present a first attempt to extend the SPT method to 3D Filippov systems. The discontinuity boundary (DB) is characterized using geometric criterions based on angular evaluations. Eighteen basic points on DB are distinguished and eight basic scenarios on DB are defined. Finally, local and global bifurcation scenarios are conceptualized with the SPT method and some illustrative examples are given.

Key–Words: Bifurcation theory, numerical analysis, non-smooth bifurcations, Filippov systems.

1 Introduction

Many engineering applications such as electric motors, power converters, brakes, gears and joints can be modelled as Filippov systems. Switchings in electrical systems [1], [2], impacting motion in mechanical systems [3], [4], stick-slip motion in oscillators with friction [5], [6], [7] and hybrid dynamics in control systems [8] are being studied with the nonsmooth dynamical systems theory.

The classical dynamical systems theory restricts the analysis to smooth phenomena such as Hopf, flip and pitchfork bifurcations and excludes the analysis of nonsmooth phenomena such as grazing, sliding and border-collision bifurcations. Understanding nonsmooth characteristics of the physical systems, we could minimize undesirable effects such as wear of components, surface damage, fatigue failure, vibration and noise [9], [10].

Figure $1(a)$ shows a block representation of many nonsmooth systems. In these systems, we can determine an energy source, an oscillator and a switching mechanism triggered by the oscillator (see figure $1(b)$) [11]. Figure $1(c)$ presents an example of sliding cycle in planar state-space where the discontinuity boundary is the line $y = 0$. The DB in 3D Filippov systems is a 2D or 3D surface; for example the plane Σ presented in figure $1(d)$.

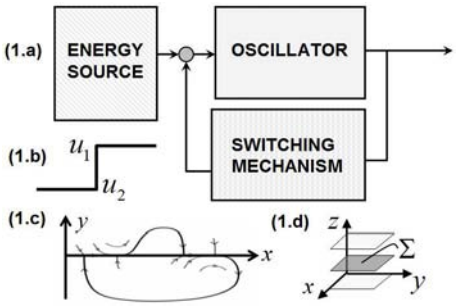

Figure 1: $(1.a)$. Generic block diagram of nonsmooth system. Three fundamental parts: Energy source, oscillator and switching mechanism. $(1.b)$. Switched signal with two positions. $(1.c)$. Example of sliding dynamic. $(1.d)$. Switching manifold or discontinuity boundary (Σ) in 3D space

Schemes of electrical and mechanical Filippov systems are presented in figure 2. The boost converter has the three elements described in figure 1. Two basic states can be distinguished: *On-state* where the inductor current increases and *Off-state* where the energy accumulated during the *On-state* is transferred to the load. Sliding dynamics can be detected when the cur-

 Manuscript Received April 29, 2008; Revised Received August 29, 2008

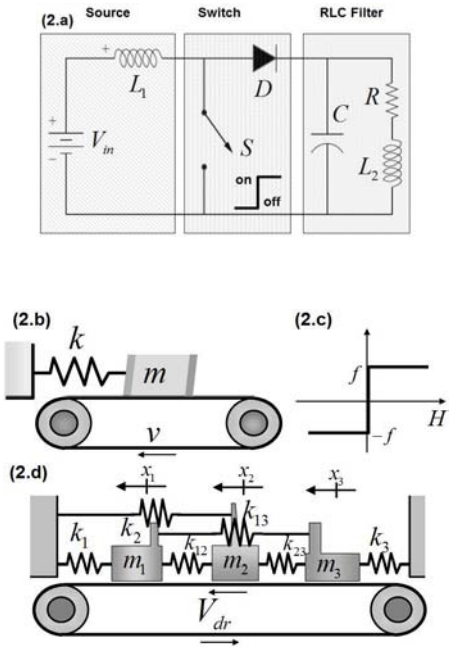

Figure 2: Examples of Filippov systems. (a). DC-DC Boost Converter (Source-Switch-Filter). (b). Undamped dry friction oscillator on a rotating belt. (c). Coulomb friction model (d). More complex mechanical system.

rent through the inductor falls to zero ($i_L = 0$).

The undamped dry friction oscillator (figure $2(b)$) comprises a block resting on a belt, moving with velocity v. The motion of block with mass m along the belt is opposed by a spring (with stiffness k) connected to a fixed support. The spring exerts a restoring force on the block that is opposed by the friction force created by the belt. When the velocity of the block is less than the velocity of the belt the friction is positive and constant and when the velocity of the block is greater than that of the belt the friction is negative. The flat Coulomb friction model is presented in figure $2(c)$. This function defines the DB as the line $y = v$.

When sliding motion on the discontinuity boundary (DB) is possible, the analysis is more complicated [12]. Moreover, the complexity can increase when the number of elements with nonsmooth interaction (as masses) is higher. An example of Filippov system with this model type is presented in figure $2(d)$.

The analysis of sliding dynamics has many mathematical and numerical difficulties. The number of specialized software in nonsmooth dynamics is reduced [13], [14]. In [15] and [6], two toolboxes are presented for analysis and continuation of nonsmooth bifurcations in Filippov systems. The platforms used in these toolboxes are Matlab and AUTO97.

A LabView toolbox was proposed in [16] for bifurcation analysis of Filippov systems denominated SPTCont 1.0. This software uses integration-free algorithms based on the evaluation of the vector fields on the discontinuity boundary (DB). The routines makes uses of the points and events classification on DB recently proposed [17], [18], [19]. Local and global bifurcations can be detected using the numerical method *Singular Point Tracking* or *SPT*. Several well-known numerical problems can be avoid using integration-free methods.

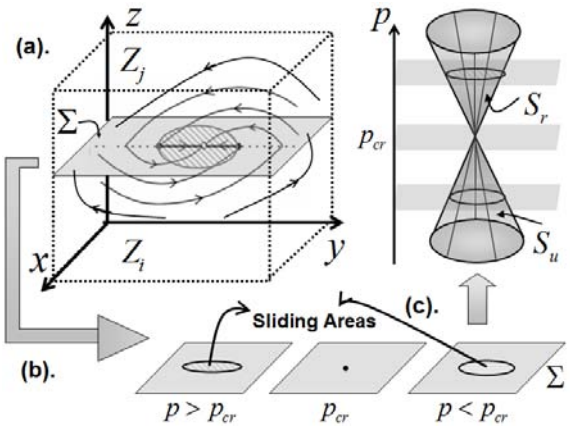

Figure 3: Example of sliding bifurcation scenario studied with SPT method. (a). $3D$ state-space, vector fields and DB. (b). Analysis of nonsmooth dynamics for different values of parameter p. (c). Generation of the bifurcation diagram and detection of the bifurcation point p_{cr}.

Planar Filippov systems have been studied extensively and many results have been studied [12], [6], [17], [20], [21], [22], [23]. In last years, the number of interesting results on local and global bifurcations in 3D systems have increased, however, many open problems persist [12].

In this paper, we present a first attempt to extend the SPT method to 3D Filippov systems. Figure 3 shows an example of sliding bifurcation scenario studied with SPT method. The 3D piecewise-smooth flows are studied on the discontinuity boundary. This analysis has two principal advantages. First, integration-free criterions can be used, therefore, the numerical errors can be reduced. Second, the dimension of the problem is reduced by one, therefore, a 3D sliding bifurcation can be detected analyzing a 2D dimensional boundary.

The discontinuity boundary (DB) is characterized using geometric criterions based on angular evaluations. The existence conditions of the *crossing areas*, *sliding areas* and *singular sliding lines* are formulate using *Boolean-valued functions* $B(.)$ based on

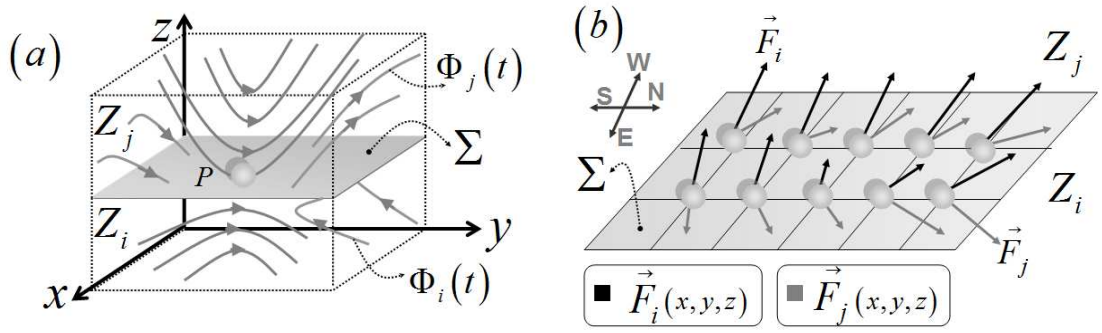

Figure 4: (a). 3D piecewise smooth state-space with two smooth flows: Φ_i and Φ_j. (b). Discontinuity boundary (2D grid) when the vector fields are evaluated in each analysis point.

integration-free geometric criterions. These conditions are easily programmable and they can be used directly in the detection of nonsmooth bifurcations.

The *Boolean-valued functions* $B(.)$ return TRUE or FALSE when their arguments are evaluated. The logical functions are composed of logical connectives: *AND*, *OR* and *NOT* denoted by $\wedge$, $\vee$ and $\neg$, respectively. Eighteen basic points on DB are distinguished and eight basic scenarios on DB are defined. Finally, local and global bifurcation scenarios are conceptualized with the SPT method and some illustrative examples are given.

The paper is organized as follows. In section II we present the background concepts of Filippov systems and the SPT numerical method. The type of areas on DB and singular lines on DB are summarized in the section III. The basic scenarios on DB are presented in the section IV while local and global bifurcation scenarios are discussed in section V. Finally, illustrative examples using SPT method are presented in section VI and the conclusions are presented in the section VII.

2 Filippov Systems and SPT method

Filippov systems are a subclass of discontinuous dynamical systems which can be described by a set of first-order ordinary differential equations with a discontinuous right-hand side [20]. These systems are modelled as piecewise-smooth systems (PWS) where the state-space contains two kinds of entities: *Smooth Zones* (Z) and *Discontinuity Boundaries* (Σ). A representation of 3D state-space is presented in figure $4(a)$.

The set of equations $\{\mathbf{F}_i(\mathbf{x}), \mathbf{F}_j(\mathbf{x}), H(\mathbf{x})\}$ given by equation (1) represents a 3D Filippov system where $\mathbf{x} \subset R^3$ and $p \in R$ is the bifurcation parameter.

$$\dot{\mathbf{x}} = \begin{cases} \mathbf{F}_i(\mathbf{x}, p) & if \quad \mathbf{x} \in Z_i \\ \mathbf{F}_j(\mathbf{x}, p) & if \quad \mathbf{x} \in Z_j \end{cases}$$
$$\Sigma = \left\{\mathbf{x} \in R^3 : H(\mathbf{x}, p) = 0\right\} \qquad (1)$$
$$Z_i = \left\{\mathbf{x} \in R^3 : H(\mathbf{x}, p) < 0\right\}$$
$$Z_j = \left\{\mathbf{x} \ \in R^3 : H(\mathbf{x}, p) > 0\right\}$$

The discontinuity boundary, (DB) denoted by Σ, is defined by the scalar function $H(\mathbf{x})$. The sign of $H(\mathbf{x})$ indicates a smooth zone that is bounded by the *DB* (figure $4(b)$). Between Z_i and Z_j the PWS system has the discontinuity boundary (DB) that it is assumed to be a smooth hyperplane.

The system (1) is not invertible because of the orbits can overlap on DB with sliding [12]. In sliding situations, a convex combination $\mathbf{G}(\mathbf{x}, \alpha)$ of the vectors $\mathbf{F}_i$ and $\mathbf{F}_j$ is defined as the Filippov Method [24].

The vector $\mathbf{G}$ can be written as the equation (2) where $0 \leqslant \lambda \leqslant 1$. The scalar product is denoted by $\langle \cdots, \cdots \rangle$.

$$\mathbf{G}(\mathbf{x}, p) = \lambda \mathbf{F}_i(\mathbf{x}, p) + (1 - \lambda)\mathbf{F}_j(\mathbf{x}, p) \qquad (2)$$

with

$$\lambda = \frac{\langle \mathbf{H}_t(\mathbf{x}), \mathbf{F}_j(\mathbf{x}) \rangle}{\langle \mathbf{H}_t(\mathbf{x}), \mathbf{F}_j(\mathbf{x}) - \mathbf{F}_i(\mathbf{x}) \rangle}$$

An analysis point P on the *DB* ($P \in \Sigma$) is defined and the vectors: $\mathbf{H}_{\Sigma W}$ and $\mathbf{H}_{\Sigma N}$ (tangent vectors to the DB in P) are computed. A perpendicular plane to Σ is defined with the vector $\mathbf{H}_{\Sigma\perp}$.

With reference to $\mathbf{H}_{\Sigma N}$, two angles θ and φ in anticlockwise direction can be associated to each 3D vector $\mathbf{F}_i$, $\mathbf{F}_j$ or $\mathbf{G}$ (see figure $5(a)$). The angles θ_i, θ_j and θ_G are computed with the projections of the vectors $\mathbf{F}_i$, $\mathbf{F}_j$ and $\mathbf{G}$ in the plane generated by the

vectors $\mathbf{H}_{\Sigma\perp}$ and $\mathbf{H}_{\Sigma N}$ (see figure $5(b)$). The angles φ_i, φ_j and φ_G are computed with the projections of the vectors $\mathbf{F}_i$, $\mathbf{F}_j$ and $\mathbf{G}$ in the plane generated by the vectors $\mathbf{H}_{\Sigma W}$ and $\mathbf{H}_{\Sigma N}$ (see figure $5(c)$).

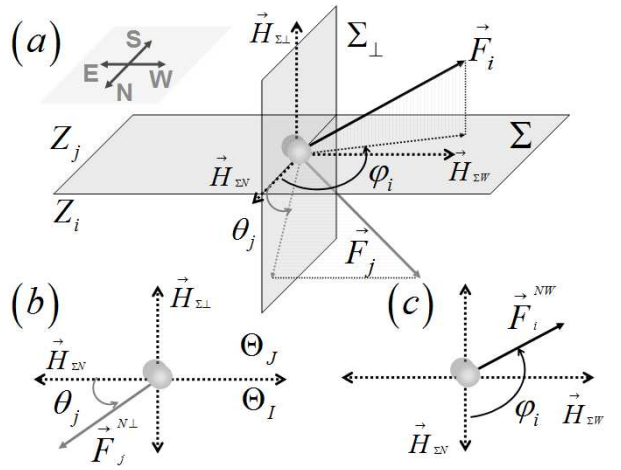

Figure 5: (a). Angular definitions (θ, φ) for each vector fields in the analysis point on DB. (b). Projection of $\mathbf{F}_j$ on $\Sigma_\perp$ plane to compute θ_j. (b). Projection of $\mathbf{F}_i$ on Σ plane to compute φ_i.

Without lost of generality and with didactic encourage supposes a dynamic system described by equation (1) and in which the perpendicular vector to the discontinuity surface is the z reference axis. Also the influence of the each vector field in the DS is equal this way

$$\dot{\mathbf{x}} = \left\{ \begin{array}{c} \mathbf{F}_i \Rightarrow F_{i,3} = F_\mu(x_1,x_2,x_3) \\ \mathbf{F}_j \Rightarrow F_{j,3} = -F_\mu(x_1,x_2,x_3) \end{array} \right\} \quad (3)$$

The solution of Filippov has been developed for nonsmooth systems where the perpendicular vectors to the trajectories have a component in the direction of the discontinuity boundary, then what we has in the inferior part of λ equation is a sum, and the result is the percentage of influence between two vector fields.

$$\lambda = \frac{F_{j,3}}{F_{j,3} + F_{i,3}} = 0,5 \quad (4)$$

and

$$\mathbf{G}(\mathbf{x}, \alpha) = \left(\frac{F_{i,1} + F_{j,1}}{2}; \frac{F_{i,2} + F_{j,2}}{2}; \right) \quad (5)$$

The made supposition converts all the discontinuity surface in a sliding area and lets to manage the dynamics of the system like smooth. As consequence it allows us to use analysis tools developed for lineal and not lineal smooth systems. This way, the results can be compared with the method SPT developed for nonsmooth systems.

In the other end, supposes that the components in the direction of the discontinuity surface changes continually and in a not synchronous way:

$$\dot{\mathbf{x}} = \left\{ \begin{array}{c} \mathbf{F}_i \Rightarrow F_{i,3} = F_\mu(\sin(x_1,x_2,x_3,\phi)) \\ \mathbf{F}_j \Rightarrow F_{j,3} = F_\omega(\sin(x_1,x_2,x_3,\phi)) \end{array} \right\} \quad (6)$$

This supposition makes the coefficient λ in a trigonometric result and transforms the discontinuity surface into a group of areas where in each, one of the four possible dynamics are presented. In this case many sliding dynamic areas are presented. Three-dimensional nonsmooth vector fields with closed forms such as spheroids, torus and warped blankets present this type of dynamics in the discontinuity surface.

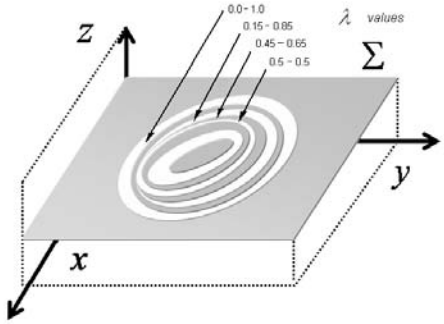

Figure 6: Equal lambda value regions in a sliding area.

Returning to Filippov solution, the coefficient λ has a value of 1 or 0 in the borders of a sliding area. In this border, λ and singular lines composed by simple tangent points are equivalent. This fact allows to determine for continuation of a singular point or unitary (or zero) λ values, the border of a sliding area. In figure 6 a discrete form of λ values of a inside sliding region of a discontinuity surface is appreciated. It is corroborated that the values inside the area are inferior to 1 and superior to 0. The border values can be only compound by 1 or 0 values depending of which is the vector field that exercises bigger influence. If the λ value is evaluated outside of a sliding area, the values do not give outstanding information and it value is always above one or below zero.

The angle φ_G of the sliding vector $\mathbf{G}(\mathbf{x})$ is used to define the direction of sliding motion in the analysis point $P \in \Sigma$.

The numerical method SPT was proposed for 2D Filippov systems [17], [18], [19]. Next we present the integration-free conditions based on angular evaluations for 3D case. With this purpose, two main ranges

of angles are defined Θ_J and Θ_I in the equation (7) where Δ_θ is the tolerance angle ($\Delta_\theta \rightarrow 0$). These ranges of angles are used to study the type of points on DB. In the figure 5 we present the ranges Θ_J and Θ_I.

$$\begin{cases} \Theta_I = \{\theta \in (\Delta_\theta, \pi - \Delta_\theta)\} \\ \Theta_J = \{\theta \in (\pi + \Delta_\theta, 2\pi - \Delta_\theta)\} \end{cases} \tag{7}$$

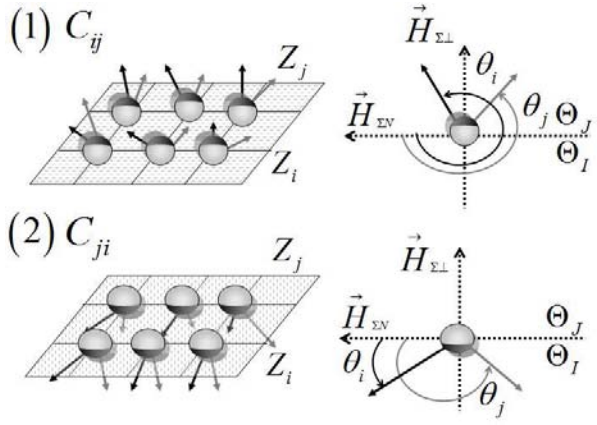

Figure 7: Crossing Areas (1) C_{ij} Area: the angles θ_i and θ_j are contained in the range Θ_J. (2) C_{ji} Area: the angles θ_i and θ_j are contained in the range Θ_I.

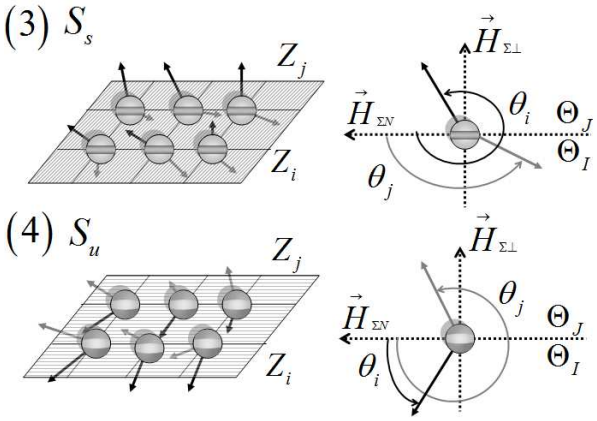

Figure 8: Sliding Areas (3) S_s Area: the angle θ_i is contained in Θ_J and θ_j is contained in the range Θ_I. (4) S_u Area: the angle θ_i is contained in Θ_I and θ_j is contained in the range Θ_J.

3 Type of Areas and Lines on 2D Discontinuity Boundary

Three types of areas can be distinguished on the discontinuity boundary (DB) in 3D Filippov Systems: *Crossing areas* (C), *Stable Sliding areas* (S_s) and *Unstable Sliding areas* (S_u). Each area is separated on DB by *singular sliding lines* (Ω).

The general *Boolean-valued conditions* $B(.)$ for the three types of areas on DB and the singular lines on DB are presented in the equation (8) where $F_i^n = \langle \mathbf{H}_n, \mathbf{F}_i \rangle$ and $F_j^n = \langle \mathbf{H}_n, \mathbf{F}_j \rangle$ are the vector field projections in the normal vector $\mathbf{H}_n$ and Q is the condition for *pseudo-equilibrium lines* given by the equation (9).

$$\begin{cases} C = B\left(F_i^n F_j^n > 0\right) \\ S = B\left(F_i^n F_j^n < 0\right) \wedge (\neg Q) \\ \Omega = B\left(F_i^n F_j^n = 0\right) \vee Q \end{cases} \tag{8}$$

$$Q = \begin{cases} B\left((\pi - \Delta_\theta) < |\theta_i - \theta_j| < (\pi + \Delta_\theta)\right) \wedge \\ B\left((\pi - \Delta_\varphi) < |\varphi_i - \varphi_j| < (\pi + \Delta_\varphi)\right) \end{cases} \tag{9}$$

Crossing and sliding flows are the predominant behaviors of the 3D Filippov systems on the discontinuity boundary (DB). Depending of the direction of the crossing orbits, two crossing (C) areas are defined and two sliding (S) areas are determined depending of the stability condition. Fourteen singular sliding lines (Ω) exist in the transition of C and S dynamics on DB.

3.1 Crossing Areas (C)

In the equation (10) we present the Boolean-valued conditions $B(.)$ for the crossing areas C_{ij} and C_{ji}. Both (θ_i and θ_j) should be contained in the same range Θ_I or Θ_J. The generic representation of the crossing areas are shown in the figure 7.

$$\begin{cases} C_{ij} = C \wedge B\left(\theta_i \in \Theta_J\right) \wedge B\left(\theta_j \in \Theta_J\right) \\ C_{ji} = C \wedge B\left(\theta_i \in \Theta_I\right) \wedge B\left(\theta_j \in \Theta_I\right) \end{cases} \tag{10}$$

3.2 Stable Sliding Areas (S_s)

In the two-dimensional case, the sliding motion was characterized according to stability and direction properties [17], [18], [19]. In the first attempt of 3D characterization, we will consider only the stability conditions.

A sliding (S) point is stable if the Boolean-valued function S_s presented in the equation (11) is `True`.

$$S_s = S \wedge B\left(\theta_i \in \Theta_J\right) \wedge B\left(\theta_j \in \Theta_I\right) \tag{11}$$

In the figure 8 (a) we present the area S_s with their respective vector fields. Note that the zenith angles should be contained in the reciprocal angle range (Θ_I or Θ_J).

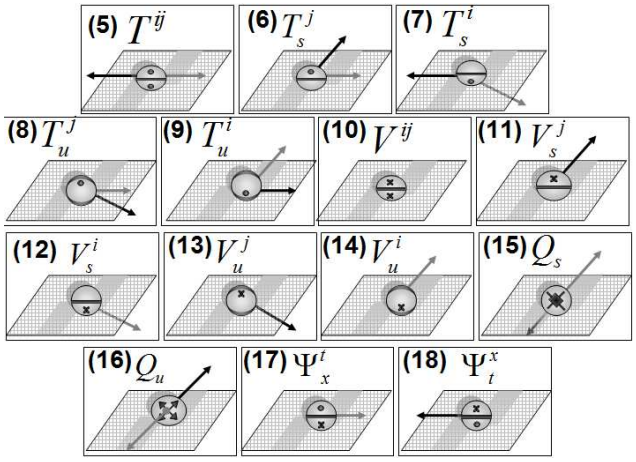

Figure 9: Singular Sliding Lines (Ω). Four classes: Tangent lines (T), Vanished lines (V), Pseudo-equilibrium lines (Q) and Tangent-Vanished lines (Ψ)

3.3 Unstable Sliding Areas (S_u)

In the same form, a sliding (S) area is unstable if the Boolean-valued function S_u presented in the equation (12) is `True`. Note that each B(.) function is excluding for each analysis point $\mathbf{x}_b$, i.e. if $C_{ij}(\mathbf{x}_b)$ is `True` then C_{ji}, S or Ω are `False` in this point. Also, if S_s is `True` in a point $P_{xy} \in \Sigma$ then S_u is `False`.

$$S_u = S \wedge B\left(\theta_i \in \Theta_I\right) \wedge B\left(\theta_j \in \Theta_J\right) \qquad (12)$$

In the figure 8 (b) we present the area S_u with their respective vector fields. The zenith angles (θ_i and θ_j) should be contained in the respective angle range (Θ_I or Θ_J).

To analyze the singular sliding points (Ω) we define four subclasses: T, V, Q and Ψ. Next, we explain the general considerations of each subclass. More details can be found in [17].

3.4 Tangent Lines (T)

The vector fields $\mathbf{F}_i$ and/or $\mathbf{F}_j$ are tangent on the analysis point $\mathbf{x}_b$. Five lines can be defined: T^{ij}, T_s^j, T_s^i, T_u^j, T_u^i. The Boolean-valued condition for Tangent (T) singular lines is given in the equation (13) where $\Theta_T = \{\theta \in (\pi/2 + \Delta_\theta, \pi/2 - \Delta_\theta)\}$(See figure 9).

$$T = \left\{ \begin{array}{c} \Omega \wedge (T_1 \vee T_2) \\ T_1 = B\left(\theta_i \in \Theta_T\right) \vee B\left(\theta_j \in \Theta_T\right) \\ T_2 = B\left(\theta_i \in \Theta_T\right) \wedge B\left(\theta_j \in \Theta_T\right) \end{array} \right. \qquad (13)$$

3.5 Vanished Lines (V)

The vector fields $\mathbf{F}_i$ and/or $\mathbf{F}_j$ are vanished on the analysis point $\mathbf{x}_b$. Five lines can be defined: V^{ij}, V_s^j, V_s^i, V_u^j, V_u^i. The Boolean-valued condition for Vanished (V) singular lines is given in the equation (14) where $\theta \notin \Theta$ implies that the magnitude of the vector field is zero ($r = 0$) (See figure 9).

$$V = \left\{ \begin{array}{c} \Omega \wedge (V_1 \vee V_2) \\ V_1 = B\left(\theta_i \notin \Theta\right) \vee B\left(\theta_j \notin \Theta\right) \\ V_2 = B\left(\theta_i \notin \Theta\right) \wedge B\left(\theta_j \notin \Theta\right) \end{array} \right. \qquad (14)$$

3.6 Pseudo-equilibrium Lines (Q)

The vector fields $\mathbf{F}_i$ and $\mathbf{F}_j$ are anti-collinear on the analysis point $\mathbf{x}_b$. Two lines can be defined: Q_s and Q_u (See figure 9). The Boolean condition was presented in the equation (9).

3.7 Tangent-Vanished Lines (Ψ)

A vector field $\mathbf{F}_i$ or $\mathbf{F}_j$ is tangent and the other vector field is vanished on the analysis point $\mathbf{x}_b$. Two lines can be defined: Ψ_x^t and Ψ_t^x (See figure 9). The Boolean-valued condition for Tangent-Vanished (Ψ) singular lines is given in the equation (15).

$$\Psi = \left\{ \begin{array}{c} \Omega \wedge (\Psi_1 \vee \Psi_2) \\ \Psi_1 = B\left(\theta_i \notin \Theta\right) \vee B\left(\theta_j \in \Theta_T\right) \\ \Psi_2 = B\left(\theta_i \in \Theta_T\right) \wedge B\left(\theta_j \notin \Theta\right) \end{array} \right. \qquad (15)$$

4 Basic Local Scenarios on DB of 3D Filippov Systems

The existence of several types of areas on the discontinuity boundary characterizes different scenarios on DB. Eight basic scenarios are considered. In all scenarios, singular sliding lines separate the crossing and sliding areas. In the figure 10 we present the characteristics of each scenario.

$$\left\{ \begin{array}{cc} (1,5,2) & (2,5,1) \\ (2,15,1) & (1,17,2) \\ (1,10,2) & (2,10,1) \\ (2,16,1) & (1,18,2) \end{array} \right\} \qquad (16)$$

– $C_{ij} \leftrightarrow C_{ji}$: Change of direction of crossing points. The singular sliding line should be: T^{ij}, V^{ij}, Q_s, Q_u, Ψ_t^x or Ψ_x^t. According to the numerical codes of the DB points, several characteristic sequences can be detected. Some examples are

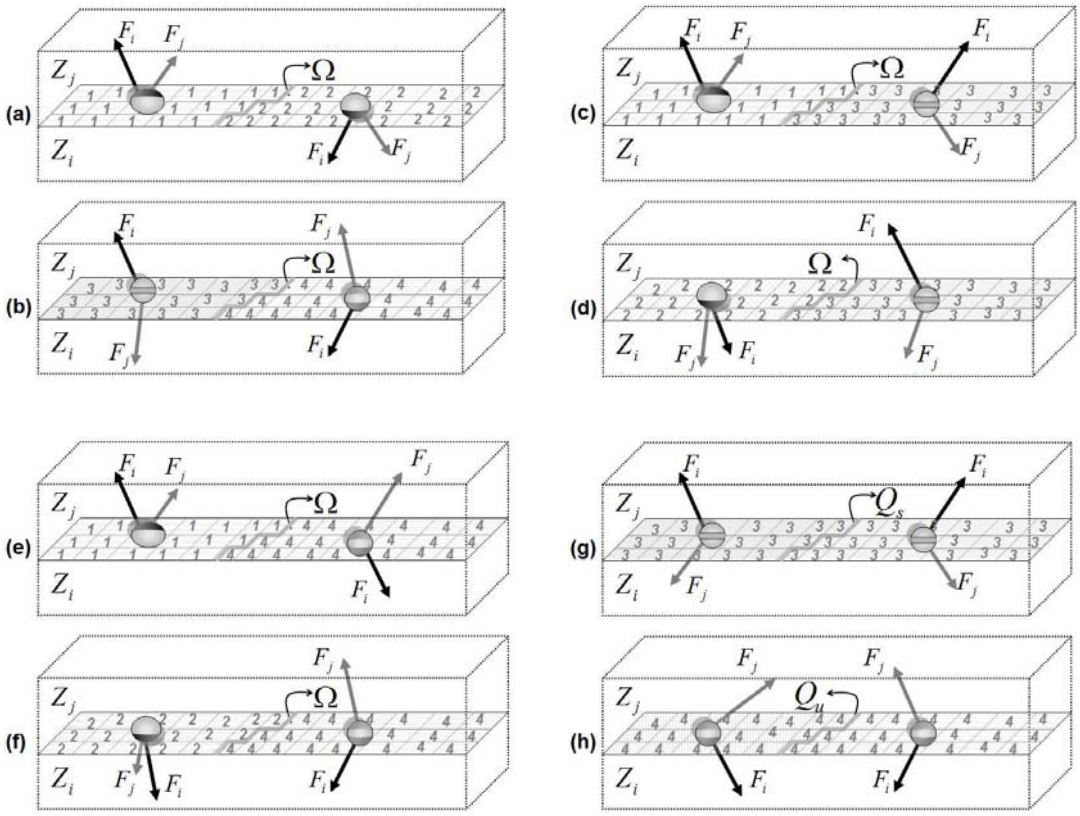

Figure 10: Examples of basic scenarios on DB in three- dimensional Filippov systems.

presented in equation (16). Figure $10(a)$ shows an example of this scenario.

$$\left\{ \begin{array}{cc} (3,5,4) & (3,17,4) \\ (4,10,3) & (4,18,3) \\ (3,10,4) & (4,17,3) \\ (4,5,3) & (3,18,4) \end{array} \right\} \tag{17}$$

– $S_s \leftrightarrow S_u$: Change of stability of sliding points. The singular sliding line should be: T^{ij}, V^{ij}, Ψ_t^x or Ψ_x^t. Some examples of characteristic sequences are presented in equation (17). Figure $10(b)$ shows an example of this case.

$$\left\{ \begin{array}{cc} (1,6,3) & (3,13,1) \\ (1,13,3) & (3,6,1) \end{array} \right\} \tag{18}$$

– $C_{ij} \leftrightarrow S_s$: Change of crossing boundary C_{ij} to stable sliding boundary and vice versa. The singular sliding line should be: T_s^j or V_s^j lines. Four characteristic sequences of this local scenario are presented in (18). Figure $10(c)$ shows an example of this scenario on DB.

$$\left\{ \begin{array}{cc} (2,12,3) & (3,7,2) \\ (2,7,3) & (3,12,2) \end{array} \right\} \tag{19}$$

– $C_{ji} \leftrightarrow S_s$: Change of crossing boundary C_{ji} to stable sliding boundary and vice versa. The singular sliding line should be: T_s^i or V_s^i lines. Four characteristic sequences of this local scenario are presented in (19). Figure $10(d)$ shows the example $(2, \Omega, 3)$.

$$\left\{ \begin{array}{cc} (1,8,4) & (4,13,1) \\ (4,8,1) & (1,13,4) \end{array} \right\} \tag{20}$$

– $C_{ij} \leftrightarrow S_u$: Change of crossing boundary C_{ij} to unstable sliding boundary and vice versa. The singular sliding line should be: T_u^j or V_u^j lines. The basic sequences are given in (20). Figure $10(e)$ shows the example $(1, \Omega, 4)$.

$$\left\{ \begin{array}{cc} (2,9,4) & (4,14,2) \\ (4,9,2) & (2,14,4) \end{array} \right\} \tag{21}$$

– $C_{ji} \leftrightarrow S_u$: Change of crossing boundary C_{ji} to unstable sliding boundary and vice versa.

The singular sliding line should be: T_u^i or V_u^i lines. The numerical sequences that SPT method should detect are given in (21). Figure $10(f)$ shows the example $(2, \Omega, 4)$.

– $S_s \leftrightarrow S_s$: Change of direction in stable sliding boundary. The singular line should be: Q_s line. The characteristic sequence of this scenario on DB is $(3, 15, 3)$. If the sliding direction is considered, this basic sequence could be decomposed in other sequences. Figure $10(g)$ shows the example $(3, 15, 3)$.

– $S_u \leftrightarrow S_u$: Change of direction in unstable sliding boundary. The singular line should be: Q_u line. The characteristic sequence of this scenario on DB is $(4, 16, 4)$. Figure $10(h)$ shows the example $(4, 16, 4)$.

5 Bifurcation scenarios on DS of 3D Filippov Systems

In nonsmooth Three-Dimensional systems in the face of the change of a parameter, the proportion areas of the different scenarios in the discontinuity surface (DS) go changing until arriving to a point where the type of scenario being presented changes generating a bifurcation that we will call bifurcation of area.

The identification of dynamics, forms and sizes of a sector in the discontinuity surface could be done using the singular point mapping method or SPT method.

The mapping method is brute force method, first it travels over all the interest discontinuity surface identifying each point type to form a map of the surface. Second, it changes a delta the value of the parameter that are been studied. The process repeats until having embraced the wanted range. The result is a 3D numeric map describing the dynamics of the surface. In figure 11 are shown four volumes with attractive and repulsive sliding dynamic and different directions.

The SPT method identifies the points belonging to the peel of the volumes and it travels them forming the volume with a low computational time consumption. It should be initialized in a singular point belonging to one of the volumes to analice. After that, it begins a continuation tracking finding equal points to initial point. After an area with a fixed parameter is swept, the parameter is varied and the process continue this way until the volume is completed.

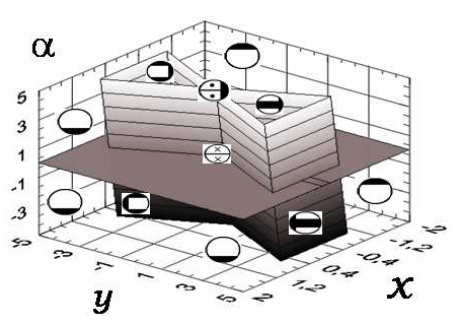

Figure 11: 3D-α representation of sliding areas as a xyα volumen.

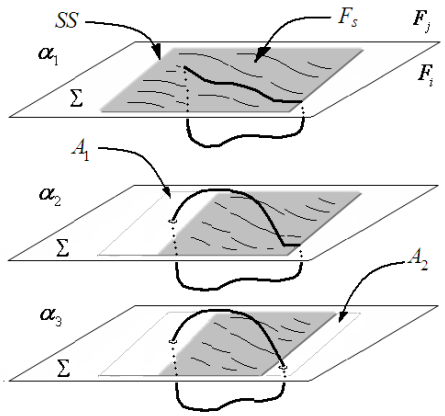

Figure 12: Global bifurcation due to sliding area size change.

5.1 Bifurcations due to changes of size or position in sliding areas

Changes in the sliding area characteristics influences the presence, disappearance or change of cycles that can leads to sliding cycle global bifurcations. In figure 12 is presented a sliding area in a decreasing sequence due to a change in a parameter that modifies the type of cycle. From the first to the second step, after disappearing the sliding area A_1, a half sliding cycle becomes a full sliding cycle and in the third step, after disappearing the sliding area A_2, it becomes a crossing cycle. The illustrative sections 6.1 presents a case where in face of a parameter change, the repulsive sliding area goes decreasing, and after disappear, it becomes attractive sliding. See figure 15.

5.2 Bifurcations due to dynamic changes in sliding areas

As we see before changes in dynamic inside a sector of the discontinuity surface affects the entere system. A special case is given when a sliding surface cap-

tures the whole dynamics. It is the case of a sliding surface with one or various stable points or limit cycles. In figure 13 is presented a case where a system is initialized from a point x_0 located in the DS. This point is crossing from F_j to F_i. For a initial value in the parameters, the trajectory in the vector field i drives the evolution toward a sliding sector in the DS. The sliding sector drives the trajectory through until abandons it in the other side. From here, a limit cycle is established. In the inferior part of the same figure it is appreciate two possible changes in the dynamics of the sliding sector. In the first one, is presented a dynamics with one stable equilibrium point. In the second, a dynamics with a limit cycle is presented. In both cases, when the trajectory entering in the sliding sector, it is caught and from now the system becomes in a two-dimensional with alone the dynamics of the sliding sector. The contrary case is also possible.

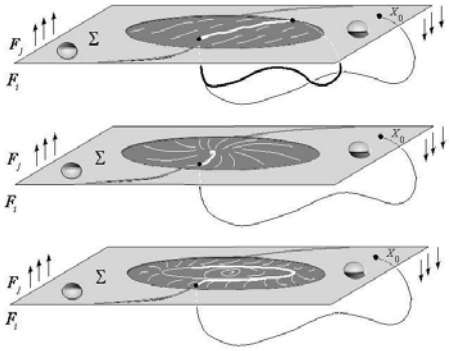

Figure 13: Extinction of three-dimensional dynamics due to stable dynamic inside sliding sector.

5.3 Bifurcations inside sliding areas

The dynamics on the DS is at least as rich as the one that is presented in a normal smooth two-dimensional system. All bifurcations presented in smooth systems are possible. Because equations representing the dynamic $\mathbf{F}_s$ in the DS are the result of the solution of Filippov, they are more complex that the original corresponding to each vector field and it opens the possibility to obtain new bifurcations. A case is presented in the example 2 of this paper. There, 3D Hopf bifurcation equations are used to define the nonsmooth system and the result is a dynamic with bifurcations no reported before.

5.4 Bifurcation of multiple sliding areas

Most of systems are compound for several elements and these interact with position restrictions. When those are being modeled give as a result multiple Discontinuity Sufaces. In each DS it is possible to find one or several of the 4 basic dynamics or complex interactions among them.

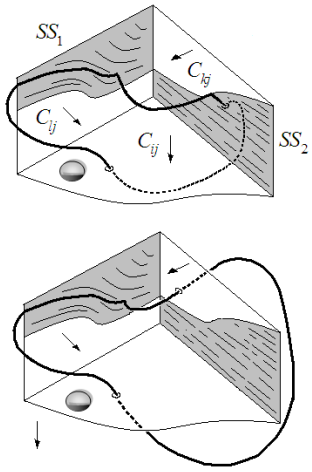

Figure 14: Vector field with various discontinuity surfaces including sliding areas.

In three-dimensional systems it is the case of the adding or multiple sliding bifurcations. These, in their simplest form abandon and return to a sliding surface, but, in their complex form they form cycles that visit several sliding surfaces. At the moment a bifurcation is give, they change the number of surfaces that are visited just as it is shown in the figure 14.

6 Illustrative examples using SPT method

6.1 Basic 3D Filippov System

Let the three-dimensional Filippov system presented in the equation (1) with the configuration $(\mathbf{F}_i, \mathbf{F}_j, H)$ given in (22).

$$\begin{aligned}
\mathbf{F}_i &= \begin{bmatrix} 0 & 0 & 1 \\ 0 & -0.2 & 0 \\ -1 & -0.1 & 0 \end{bmatrix} \begin{bmatrix} x \\ y \\ z \end{bmatrix} + \begin{bmatrix} 0 \\ 0 \\ \alpha \end{bmatrix} \\
\mathbf{F}_j &= \begin{bmatrix} 0 & 0 & 1 \\ 0 & -0.2 & 0 \\ -1 & -0.1 & 0 \end{bmatrix} \begin{bmatrix} x \\ y \\ z \end{bmatrix} + \begin{bmatrix} 0 \\ 0 \\ -\alpha \end{bmatrix} \qquad (22) \\
H &= z
\end{aligned}$$

The configuration (22) can be found in mechanical systems as friction oscillators where α is the bifurcation parameter. In the figure 15, the sliding areas

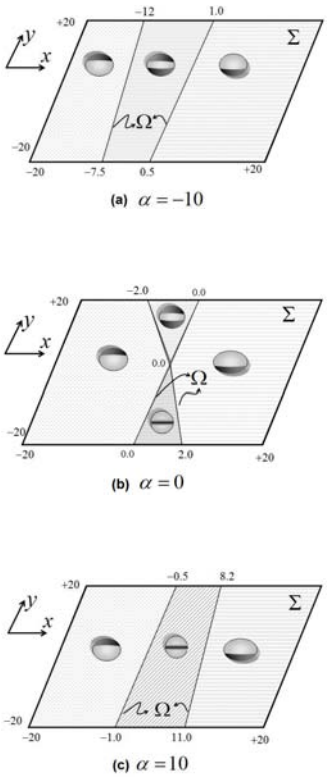

Figure 15: Illustrative Example. Crossing and sliding areas on DB of 3D Filippov System.

are presented in the plane xy bounded by $x = \pm 20$ and $y = \pm 20$.

For $\alpha < 0$ (figure 15 (a)), the DB has crossing areas and unstable sliding areas. For $\alpha = 0$ (figure 15 (b)), the system has a DB where the sliding area S_s appears. For $\alpha > 0$ (figure 15 (c)), the system has a DB where the unstable sliding area disappears.

6.2 Parametric bifurcations on DS based in 3D Hopf bifurcation dynamic

In this section the objective is to show the richness dynamic in the discontinuity surface between vector fields when exist sliding in a sector. The studied systems is a 3D system with equal equation structure that equation (3) and described by the vector field $\dot{\mathbf{x}}$ with the following equations:

$$\dot{\mathbf{x}} = \left\{ \begin{array}{c} F_{i,1}; F_{i,2}; F_{i,3} \\ F_{j,1}; F_{j,2}; F_{j,3} \end{array} \right\} \tag{23}$$

with F_1, F_2 y F_3

$$\left[\begin{array}{c} F_1 \\ F_2 \\ F_1 \end{array} \right] = \left[\begin{array}{c} = \psi_1(x_1+\alpha) + \delta_1(x_2+\beta) + \\ \sigma(x_1+\alpha)\left[(x_1+\alpha)^2 + (x_2+\beta)^2\right] \\ = \psi_2(x_2+\beta) - \delta_2(x_1+\alpha) + \\ \sigma(x_2+\beta)\left[(x_1+\alpha)^2 + (x_2+\beta)^2\right] \\ = \kappa_1 \end{array} \right] \tag{24}$$

In the event of not having a computational tools that work directly with nonsmooth systems you can welcome to the simplification mentioned in the section 2 making $F_{i3} = -F_{j3}$ and $\mathbf{F}_s$ equal to:

$$\mathbf{F}_s * 2 = \left[\begin{array}{c} = F_{i1} + F_{j1} \\ = F_{i2} + F_{j2} \end{array} \right] \tag{25}$$

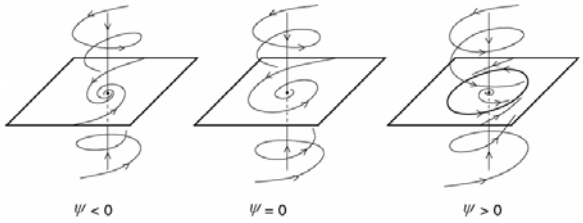

Figure 16: Free dynamic of 3D Hopf bifurcation in a smooth system.

For each vector field i and j, the parameter ψ determines the stability. When ψ has a value equal to zero as it is presented in the figure 6.2 a Hopf bifurcation is presented. For values of ψ over zero the dynamics forms a limit cycle with radio equal to the square root of ψ. The CW or CCW turn is determined by the parameter δ. The advance orientation of the hairspring in the z direction is determined by the sign of the parameter κ. If $\kappa > 0$ the advance is the positive direction of z. The parameters α and β determine the displacement of the dynamics in the xy plane.

$$\dot{\mathbf{x}} = \left\{ \begin{array}{c} \mathbf{F}_i(\mathbf{x}, \alpha, \beta, \psi, \delta, \sigma, \kappa > 0) \\ \mathbf{F}_j(\mathbf{x}, \alpha, \beta, \psi, \delta, \sigma, \kappa < 0) \end{array} \right\} \tag{26}$$

As it is appreciated in the equations (24), (23)y (26), the answer of the system is only conditioned by the values of the parameters. The following initials values are selected and changes of its values has been plotted versus the stability characteristics.

$$\dot{\mathbf{x}} = \left\{ \begin{array}{l} \mathbf{F}_i(\alpha = \beta = 0, \psi_1 = \psi_2 = 4, \\ \delta = 1, \sigma = -1, \kappa = 0,01) \\ \mathbf{F}_j(\alpha = \beta = 0, \psi_1 = \psi_2 = 9, \\ \delta = 1, \sigma = -1, \kappa = -0,01) \end{array} \right\} \tag{27}$$

6.2.1 Vector fields i and j with limit cycles

With the initial values, the result is a limit cycle with trajectory between those original vector fields would form over the discontinuity surface. See figure 17. The λ value determines the proximity to anyone of the two original vector field.

Figure 17: Resulting trajectory of a nonsmooth system with limit cycles vector fields.

- for equal values of $\psi_{1\mathbf{i}}$,$\psi_{1\mathbf{j}}$,$\psi_{2\mathbf{i}}$ and $\psi_{2\mathbf{j}}$, the results are limit cycles C_1, C_2, C_3 with diameter equal to the ψ root.
- for values of $\psi_{1\mathbf{i}}$ equal to $\psi_{2\mathbf{i}}$ and $\psi_{2\mathbf{i}}$ equal to $\psi_{2\mathbf{j}}$, the results are:
  - Limit Cycles with trajectories in which dynamics speed varies depending of ubication in space state. When trajectory passes the original cycles intersection, smaller speeds are presented. Points E and D in the figure 18 indicate sectors with low speed. These correspond to values of $\psi_{1\mathbf{i}}$ equal to 7.5 and $\psi_{2\mathbf{i}}$ equal to 6.5 and vice versa
  - Three equilibrium points, two of them stables and one unstable in intermediate position. Points A and B with values of $\psi_{1\mathbf{i}}$ equal to 9.0 and $\psi_{2\mathbf{i}}$ equal to 4.0 and vice versa. Between previous item and this one, a bifurcation is presented starting with limit cycle and ending with three equilibrium points.

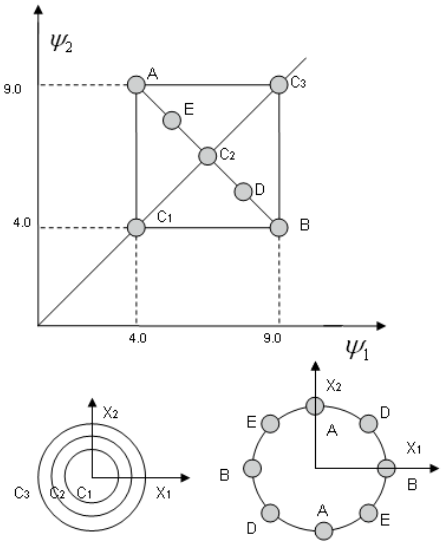

Figure 18: Changes in size and final stabilization point in relation with ψ parameter.

- For values $\delta_1 = -\delta_2$ and equal conditions that the initial ones, it is formed a fictitious cycle where all trajectories converge but once they arrive to any point of this cycle, they stop forming a stable point. This situation corresponds to the diagonal line in figure 19. The location of equilibrium points in the fictitious cycle depends of their parameter values.

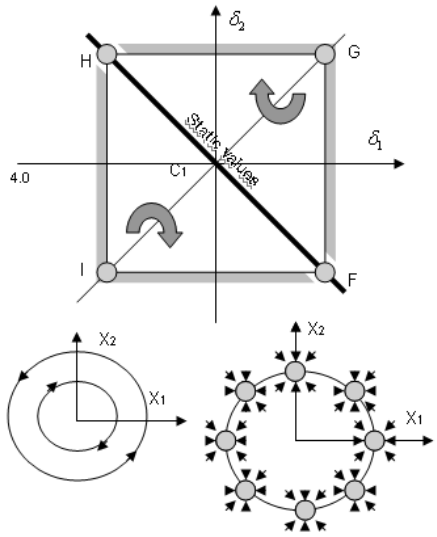

Figure 19: Changes in direction and final stabilization point in relation with δ parameter.

- For values $\delta_1 \neq \delta_2$, it is formed in figure 19 two sectors where in each one, limit cycles are pre-

sented but with different turn sense. Limit cycle speed depends of distance from the parameter static line in the figure 19.

- For α and β values where $\psi_{1,2,\mathbf{i},\mathbf{j}}$ are equal to 9.0 and $\rho = \sqrt{\alpha^2 + \beta^2}$, three stability types are presented:
  - For ρ values smaller than 2.4 a limit cycle is presented. With low values, the cycles are perfect but as ρ is increased, they change speed and become deformed until arriving to the value where the bifurcation is given.
  - For ρ values between 2.4 and 3.0 three equilibrium points with two stable points and one unstable point are presented. When ρ is close to 3.0 both points become closer.
  - For ρ values bigger than 3.0 only one equilibrium point is presented.

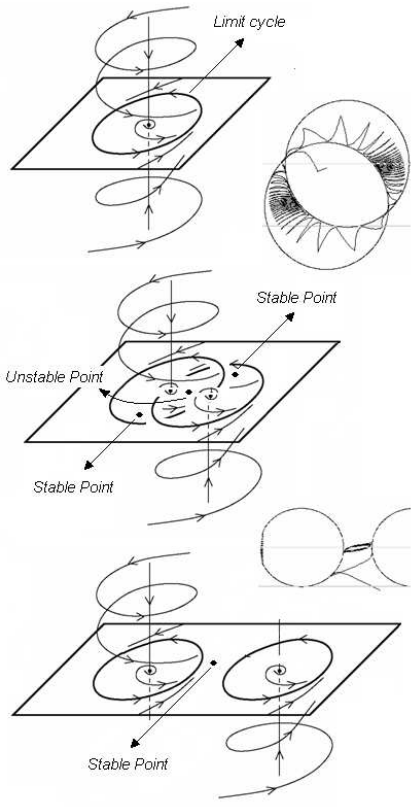

Figure 20: Bifurcation due to value changes of α and β parameter.

The phase portraits sequence presented in the face of parameter changes has not topological equivalence and therefore this is a nonsmooth bifurcation type that had not been reported until the moment. In figure 20 is shown and schematic sequence and some appearances of integration with big step-size and Filippov solution disabled to observe the tendency of each vector field.

6.2.2 Vector field i with stable dynamic and vector field j with limit cycle

- For $\psi_{1\mathbf{i}}$ and $\psi_{2\mathbf{i}}$ values smaller that zero, limit cycles are presented . When the negative absolute values of $\psi_{1\mathbf{i}}$ and $\psi_{2\mathbf{i}}$ are higher that the positive values of $\psi_{1\mathbf{j}}$ and $\psi_{2\mathbf{j}}$, the system presents a stable point located according to the alpha and beta parameter values.

7 Conclusions

We have presented the numerical analysis of sliding dynamics on the discontinuity boundary (DB) of three-dimensional Filippov systems using an integration-free method denominated Singular Point Tracking (SPT). The discontinuity boundary (DB) has been characterized using geometric criterions based on angular evaluations. Eighteen basic points on DB have been distinguished and eight basic scenarios on DB have been defined. Finally, local and global bifurcation scenarios have been conceptualized with the SPT method.

Future work will address the generalization of SPT method to different 3D sliding bifurcation scenarios. Later, the future work will address the analysis of higher-dimensional Filippov systems with more general vector fields.

References:

[1] B. Brogliato. *Nonsmooth Mechanics Models, Dynamics and Control*. Springer Verlag, New York, 1999.

[2] C. J. Budd M. di Bernardo and A. R Champneys. Grazing and border−collision in piecewise smooth systems: a unified analytical framework. *Phys. Rev. Lett*, 86:2553,2556, 2001.

[3] R. Alzate M. di Bernardo S. Santini, U. Montanaro. Experimental and numerical verification of bifurcations and chaos in cam−follower impacting systems. *to appear in Nonlinear Dynamics (DOI 10.1007/s11071-006-9188-8)*, 2007.

[4] P. Kowalczyk and M. di Bernardo. Two−parameter degenerate sliding bifurcations in filippov systems. *Physica D−Nonlinear Phenomena*, 204(3-4):204229, May 2005.

[5] B. Brogliato. *Impacts in Mechanical Systems Analysis and Modelling*. Springer Verlag, New York. Lecture Notes in Physics, Volume 551., 2000.

[6] F. Dercole Yu. A. Kuznetsov. Slidecont: An auto97 driver for bifurcation analysis of filippov systems. *ACM Trans. Math. Softw*, 31, 95−119, 2005.

[7] S. Khanmohamadi A. Ghanbari. A new test rig for frictional torque measurement in ball bearings. *WSEAS TRANSACTIONS on SYSTEMS, Issue 9, Volume 5*, September 2006.

[8] N. Zanzouri A. Zaidi and M. Tagina. Graphical approaches for modelling and diagnosis of hybrid dynamic systems. *WSEAS TRANSACTIONS on SYSTEMS, Issue 10, Volume 5*, October 2006.

[9] A B Nordmark. Existence of priodic orbits in grazing bifurcations of impacting mechanical oscillators. *Nonlinearity*, 14:15171542, 2001.

[10] U. Galvanetto. Some discontinuous bifurcations in a two−block stick−slip system. *Journal of Sound and vibration*, 248(4), 653−669, 2001.

[11] K. Popp and P. Stelter. Stick-slip vibrations and chaos. *Philosophical Transactions: Physical Sciences and Engeneering*, 332(1624):89–105, July 1990.

[12] Yu. A. Kuznetsov S. Rinaldi, A. Gragnani. One−parameter bifurcations in planar filippov systems. *International Journal of Bifurcations and Chaos*, 13(8):21572188, 2003.

[13] P. Mosterman and G. Biswas. A theory of discontinuities in physycal system models. *El Sevier*, 325B, 1998.

[14] Sven Hedlund. *Computational Methods for Hybrid Systems*. PhD thesis, Lund Institute of Technology, 1999.

[15] P.T. Piiroinen Yu. A. Kuznetsov. An event−driven method to simulate filippov systems with accurate computing of sliding motions. *Technical report, University of Bristol*, 2005.

[16] I. Arango and J. A. Taborda. Sptcont 1.0: A labview toolbox for bifurcation analysis of filippov systems. *Proceedings of the 12th WSEAS International Conference on Systems, Heraklion, Greece*, 2008, pp. 587–595.

[17] I. Arango J. A. Taborda. Integration-free analysis of nonsmooth local dynamics in planar filippov systems. *International Journal of Bifurcation and Chaos, to appear*, 19(3), March 2009.

[18] I. Arango and J. A. Taborda. Characterizating points on discontinuity boundary of filippov systems. *Proceedings of IASTED International Conference on Modelling, Identification and Control (MIC 2008)*, 2008, Innsbruck, Austria.

[19] I. Arango and J. A. Taborda. Analyzing sliding bifurcations on discontinuity boundary of filippov systems. *Proceedings of the American Conference on Applied Mathematics (MATH 08), Cambridge USA*, 2008, pp. 165–170.

[20] Leine R.I. H. Nijmeijer. *Dynamics and Bifurcations in Non − Smooth Mechanical Systems*. Springer Verlag, 2004.

[21] Albert C.J. Luo. A theory for non−smooth dynamic systems on the connectable domains. *Communications in Nonlinear Science and Numerical Simulation*, 10 1−55, 2005.

[22] A.R. Champneys S.J. Hogan M. Homer Yu.A. Kuznetsov A. Nordmark P. Kowalczyk, M. di Bernardo and P.T. Piiroinen. Two−parameter nonsmooth bifurcations of limit cycles: classification and open problems. *International Journal of Bifurcations and Chaos*, 2006.

[23] J. A. Ferreira. A review of mathematical models of non-linear mechanical systems that involve friction. *WSEAS TRANSACTIONS on SYSTEMS, Issue 12, Volume 6*, December 2007.

[24] A. F. Filippov. Differential equations with discontinuous righthand sides. *Kluwer Academic Publishers*, Dortrecht, 1988.